Natural Resources for Human Health
eISSN: 2583-1194

Original Research

Received 31 May 2026
Revised 14 July 2026
Accepted 28 July 2026

Natural Resources for Human Health 2026, Vol. 6 (13s): 509–526

KEYWORDS:
Fenofibrate; Nanosponges; Colon-targeted drug delivery; Box–Behnken design; Pharmacokinetics; DSS-induced colitis; Inflammatory bowel disease; PPAR-α; Anti-inflammatory.

Fenofibrate Colon-Targeted Nanosponges Development, Optimization, and In-Vivo Anti-Inflammatory Efficacy of Fenofibrate Nanosponges: A Box–Behnken Design Approach to Formulation, Pharmacokinetics, and Experimental Colitis

Ramya Teja Medarametla 1,Gadela Venkata Radha2 *

1 Department of Pharmaceutics, GITAM School of Pharmacy, GITAM (Deemed to be University), Visakhapatnam, Andhra Pradesh, INDIA
2* Department of Pharmaceutics, GITAM School of Pharmacy, GITAM (Deemed to be University), Visakhapatnam, Andhra Pradesh, INDIA radhagadela@gmail.com

ABSTRACT: Background: Fenofibrate, a PPAR-α agonist with anti-inflammatory, lipid-modulating and lipid-lowering properties, is limited clinically by poor aqueous solubility and low oral bioavailability, restricting its use for inflammatory bowel disease (IBD). This study aimed to develop and optimize fenofibrate nanosponge formulation to improve drug solubility, achieve sustained colonic delivery, and enhance pharmacokinetic performance, and subsequently to evaluate the in-vivo anti-inflammatory and lipid-modulating efficacy of this optimized platform in dextran sulfate sodium (DSS)-induced experimental colitis.

Methods: Fenofibrate-loaded β-cyclodextrin nanosponges were prepared by the solvent evaporation method using diphenyl carbonate as crosslinker. A three-factor, three-level Box–Behnken design (BBD) was employed to optimize polymer concentration, crosslinker:polymer ratio, and stirring time, using particle size, entrapment efficiency, drug release, and zeta potential as responses. The optimized formulation was characterized by FTIR, DSC, XRD and scanning electron microscopy, and evaluated for in-vitro release and release kinetics, in-vivo pharmacokinetics in Wistar rats, and accelerated/long-term stability. The same optimized formulation was then evaluated for in-vivo anti-inflammatory and lipid-modulating efficacy in a DSS-induced colitis model in male BALB/c mice (normal control, DSS control, fenofibrate suspension 100 mg/kg, and fenofibrate nanosponge 100 mg/kg groups, treated on days 8–17), assessing serum lipid parameters, colonic inflammatory cytokines (TNF-α, IL-1β, IL-6, IL-10), and colonic histopathology, with the in-vivo design and reporting aligned with the ARRIVE 2.0 guidelines.

Results: The quadratic models for all four formulation responses were statistically significant ($p \leq 0.0004$), with the crosslinker:polymer ratio identified as the predominant factor. The optimized formulation showed a particle size of 183.42 nm, entrapment efficiency of 89.76%, drug release of 78.63% at 10 h, and zeta potential of −29.88 mV, with prediction errors below 1%. FTIR, DSC and XRD confirmed drug–polymer compatibility with reduced fenofibrate crystallinity, and SEM revealed a porous nanosponge architecture. The formulation exhibited pH-dependent sustained release (Korsmeyer–Peppas, Super Case II transport) and improved pharmacokinetic parameters

(higher Cmax, AUC and mean residence time) relative to pure drug suspension, with no significant change in physicochemical properties over six months of stability testing. In the DSS-colitis model, DSS administration induced significant dyslipidemia and elevated the pro-inflammatory cytokines TNF-α, IL-1β and IL-6 while reducing IL-10, together with marked crypt distortion, epithelial erosion, and inflammatory infiltration on histopathology. Treatment with the fenofibrate nanosponge restored serum lipid parameters toward normal, significantly reduced TNF-α, IL-1β and IL-6, restored IL-10, and preserved colonic mucosal architecture with near-normal crypts and goblet cells, with effects comparable to or exceeding plain fenofibrate suspension and mesalamine.

Conclusion: A colon-targeted fenofibrate nanosponge formulation was successfully optimized using Box–Behnken design, demonstrating nanoscale particle size, high entrapment efficiency, pH-dependent sustained release, favorable stability, and improved oral bioavailability compared with pure fenofibrate. This optimized delivery platform translated into promising in-vivo anti-inflammatory and lipid-modulating efficacy in DSS-induced experimental colitis, supporting its therapeutic potential as a colon-targeted delivery system for inflammatory bowel disease.

INTRODUCTION

Fenofibrate is a well-established peroxisome proliferator-activated receptor-alpha (PPAR-α) agonist, widely used for its lipid-lowering activity and increasingly explored for pleiotropic anti-inflammatory and immunomodulatory effects that make it a candidate for local, colon-targeted delivery [1]. It modulates key inflammatory pathways, including downregulation of pro-inflammatory cytokines such as tumor necrosis factor-alpha (TNF-α), interleukin-1 beta (IL-1β), and interleukin-6 (IL-6), while promoting the anti-inflammatory mediator interleukin-10 (IL-10) [8,9]. However, its clinical utility is significantly hindered by poor aqueous solubility, limited oral bioavailability, and rapid hepatic metabolism, resulting in insufficient drug concentrations at the target site within the colon. These pharmacokinetic limitations necessitate innovative drug delivery strategies capable of enhancing solubility while achieving site-specific, sustained release.

Inflammatory bowel disease (IBD), comprising Crohn's disease and ulcerative colitis, is a chronic, relapsing inflammatory disorder of the gastrointestinal tract driven by an imbalance between pro- and anti-inflammatory cytokines, leading to persistent mucosal inflammation, tissue damage, and impaired intestinal barrier function [2]. Its etiology involves complex interactions among genetic predisposition, environmental factors, immune dysregulation, and gut microbiota alterations [3]. Despite advances in understanding its pathophysiology, current therapeutic options remain limited by suboptimal drug solubility, poor bioavailability, rapid systemic clearance, and adverse side effects, which collectively impede effective disease management and patient compliance [4]. Fenofibrate's pleiotropic anti-inflammatory effects therefore position it as a promising candidate for adjunct therapy in IBD, provided its colonic bioavailability can be sufficiently improved [8,9].

Nanosponges, a novel class of porous, nanoscale carriers, have emerged as an effective platform for improving drug solubility, stability, and controlled release. Their unique three-dimensional network structure enables high drug-loading capacity and protects labile drugs from premature degradation [5]. β-Cyclodextrin-based nanosponges, in particular, offer additional advantages due to their biocompatibility, ability to form inclusion complexes, and selective targeting potential [6], making them well suited to colon-targeted delivery applications that require higher local drug concentrations while minimizing systemic exposure [7].

This study was accordingly designed in two integrated stages, together forming a complete evaluation of the formulation from bench to therapeutic proof-of-concept. First, fenofibrate-loaded β-cyclodextrin nanosponges were developed and optimized for colon-targeted delivery using a three-factor, three-level Box–Behnken design, and the optimized formulation was thoroughly characterized using dynamic light scattering, FTIR, DSC, XRD and scanning electron microscopy, with in-vitro release studies performed to elucidate the drug release mechanism and in-vivo pharmacokinetic and stability evaluations conducted to assess bioavailability and shelf-life performance relative to pure fenofibrate. Second, building on this optimized platform, the in-vivo anti-inflammatory and lipid-modulating efficacy of the fenofibrate nanosponge was evaluated using a dextran sulfate sodium (DSS)-induced colitis model in mice [10], a well-established experimental paradigm that mimics key pathological features of

human IBD, with serum lipid profiles, colonic inflammatory cytokines, and histopathological changes examined, and the in-vivo experimental design and reporting aligned with the ARRIVE 2.0 guidelines [11], to determine whether colon-targeted, sustained delivery translates into superior anti-inflammatory and lipid-modulating efficacy compared with plain fenofibrate.

MATERIALS AND METHODS

Chemicals and Reagents

Fenofibrate was procured from Yarrow Chem Products, Mumbai, India (purity >98% by GC). β-Cyclodextrin and diphenyl carbonate were obtained from Sigma-Aldrich (Merck, India). Ethanol, phosphate-buffer reagents and other analytical-grade chemicals were obtained from Merck/SRL, India. HPLC-grade solvents were used for analytical studies. All chemicals were used as received without further purification.

Experimental Design

Design-Expert (DoE optimization)

The optimisation of nanosponges was carried out with three factors at three levels, using a Box–Behnken design (BBD). The independent variables were polymer concentration, crosslinker:polymer ratio, and stirring time (Table 1). The dependent variables (responses) were particle size, entrapment efficiency, drug release, and zeta potential (Table 2). Seventeen runs were obtained using STAT-EASE 360 trial version software (Table 3). A quadratic equation was used to study the effect of factors on responses:

Response = $b0 + b1A + b2B + b3C + b12AB + b13AC + b23BC + b11A^2 + b22B^2 + b33C^2$, where b0 is an intercept; b1 to b33 are regression coefficients derived from the dependent variables; and A, B, and C are the independent variables.

Table 1. Independent Variables (Factors)

Factors	Coded levels	Actual levels
Polymer concentration (A) (%w/v)	Low (−1) – Medium (0) – High (+1)	2 – 4 – 6
Crosslinker: polymer ratio (B) (%w/w)	Low (−1) – Medium (0) – High (+1)	2:1 – 4:1 – 6:1
Stirring time (C) (hours)	Low (−1) – Medium (0) – High (+1)	2 – 4 – 6

Table 2. Dependent Variables (Responses)

Responses	Goal
Particle size (nm)	Minimum
Entrapment efficiency (%)	Maximum
Drug release (%)	Controlled
Zeta potential (mV)	Optimize stability

Preparation of Fenofibrate-Loaded Nanosponges

Fenofibrate-loaded nanosponges were prepared by the solvent evaporation method. Briefly, fenofibrate and β-cyclodextrin were dissolved in 25 mL of ethanol to obtain a homogeneous organic phase. Diphenyl carbonate was dissolved separately to prepare the crosslinking solution. The organic phase was added slowly to 75 mL of the aqueous phase under continuous magnetic stirring at 1000 rpm. Polymer concentration, crosslinker-to-polymer ratio, and stirring duration were varied according to the Box–Behnken experimental design. During stirring, solvent evaporation facilitated crosslinking between β-cyclodextrin and diphenyl carbonate, resulting in porous nanosponge structures encapsulating fenofibrate. After complete evaporation of the solvent, the nanosponges were collected, dried at room temperature, and stored in a desiccator until further characterization. Seventeen formulations were prepared according to the experimental design; the optimized formulation was subsequently filled into Eudragit S100 to confer pH-dependent, colon-targeted release.

Table 3. Formulation Table of Runs

Run	Fenofibrate (mg)	β-CD (% w/v)	β-CD (g)	Crosslinker: Polymer Ratio	Diphenyl Carbonate (g)	Stirring Time (h)
1	100	4	4	2:1	2.0	6
2	100	4	4	2:1	2.0	2
3	100	2	2	4:1	0.5	2
4	100	4	4	4:1	1.0	4
5	100	6	6	6:1	1.0	4
6	100	4	4	4:1	1.0	4
7	100	4	4	4:1	1.0	4
8	100	4	4	4:1	1.0	4
9	100	6	6	2:1	3.0	4
10	100	2	2	4:1	0.5	6
11	100	6	6	4:1	1.5	6
12	100	4	4	4:1	1.0	4
13	100	4	4	6:1	0.67	6
14	100	2	2	2:1	1.0	4
15	100	2	2	6:1	0.33	4
16	100	6	6	4:1	1.5	2
17	100	4	4	6:1	0.67	2

Characterization of Fenofibrate-Loaded Nanosponges

Particle size analysis, PDI, and zeta potential

Particle size was determined using a dynamic light scattering (DLS) technique with a Zetasizer operated at 25°C. Each formulation was dispersed in distilled water and sonicated for 5 min before measurement. The hydrodynamic diameter was calculated based on the Stokes–Einstein equation, with measurements performed at a scattering angle of 90°. The surface charge of the optimized nanosponge formulation was measured using a Zetasizer at 25°C without dilution (1.2 mL) using single-use cuvettes (disposable folded capillary cell – DTS1070). All measurements of particle size, PDI, and zeta potential were performed in triplicate.

Entrapment efficiency

Entrapment efficiency was determined by measuring the amount of unentrapped drug after centrifugation. Nanosponges equivalent to 10 mg of fenofibrate were dispersed in phosphate buffer (pH 7.4) and centrifuged at 15,000 rpm for 30 min. The concentration of free drug in the supernatant was quantified spectrophotometrically (UV-1900i, Shimadzu) at 290 nm. Entrapment efficiency (%) was calculated as [(Total drug − Free drug) / Total drug] × 100, where Total drug represents the initial amount of drug used in the formulation and Free drug represents the amount of unentrapped drug measured in the filtrate.

In-vitro drug release and release kinetics

The Eudragit S100-coated capsules were evaluated for drug release using a dissolution apparatus at 37°C at 50 rpm. Drug release

was tested at pH 1.2 (for 2 hours), 6.8 (for 3 hours), and 7.4 (for 5 hours). Samples were withdrawn at predetermined intervals and analyzed spectrophotometrically, and the cumulative percentage drug release was calculated for each formulation.

Solubility and dissolution studies of fenofibrate and optimized nanosponge formulation

An excess quantity of drug was added to 10 mL of distilled water and shaken for 24 hours. The samples were centrifuged, and the supernatant was suitably diluted with pH 7.4 phosphate buffer. Samples were analysed using a UV-Vis spectrophotometer to determine drug quantity; the procedure was repeated for the optimized formulation. The dissolution study was conducted using a USP type II dissolution apparatus at 37 ± 0.5°C at 50 rpm. An accurately weighed quantity of pure drug and optimized formulation containing the same quantity of drug was introduced into 900 mL of distilled water. 5 mL samples were withdrawn at 5, 10, 20, 30, 45, 60, 90 and 120 min, with an equal volume of distilled water replaced after each withdrawal. The withdrawn samples were suitably diluted with pH 7.4 phosphate buffer and analysed spectrophotometrically.

Physicochemical Characterization of the Optimized Formulation

FTIR studies were conducted to identify the functional groups of fenofibrate and to assess possible interactions between the drug and the excipients. Samples were dispersed in KBr and pressed into pellets, and analysed using an FTIR spectrophotometer (Bruker, Germany) over the range of 4000–400 cm^{-1}. DSC studies were performed using a differential scanning calorimeter (STA-7300, Hitachi, Germany) on fenofibrate and the optimised formulation to determine thermal behaviour; samples were heated from 25°C to 300°C under a nitrogen atmosphere at 10°C/min, and thermograms were recorded as heat flow (mW) versus temperature (°C). XRD studies were conducted using an X-ray diffraction unit (PANalytical) to determine the crystalline nature of fenofibrate and any changes induced by the nanosponge formulation, with diffraction patterns recorded using Cu-Kα radiation over the 2θ range.

Morphological Analysis

The surface morphology of the optimized nanosponge formulation was examined using scanning electron microscopy (SEM). Samples were mounted on aluminum stubs, coated with a conductive metal layer, and examined under appropriate accelerating voltage to evaluate particle morphology, surface texture, porosity, and nanosponge architecture.

Optimization and Validation

Numerical optimization was carried out using the desirability function approach in Design-Expert® software. The optimized formulation was selected by minimizing particle size while maximizing entrapment efficiency and maintaining controlled drug release and desirable zeta potential. The optimized formulation was prepared independently, and the observed responses were compared with predicted values to validate the model; the percentage prediction error was calculated to assess model reliability.

Pharmacokinetic Study

The in-vivo pharmacokinetic study was carried out to evaluate the bioavailability of the optimized fenofibrate nanosponge formulation compared to a fenofibrate suspension. The study was done in Wistar rats of weight 200–250 g, following ethical approval (IAEC: 1292/ac09/CPCSEA/2021/3). Rats were fasted overnight with access to water before dosing and grouped into two (n = 6): Group I received the fenofibrate suspension and Group II received the optimized formulation at an equivalent dose (10 mg/kg). Blood samples were collected via the retro-orbital plexus at predetermined intervals (0, 1, 2, 3, 4, 5, 6, 7, 8, 9, 10 h), centrifuged at 5000 rpm for 10 min at 4°C to obtain plasma, and stored at −20°C until analysis. Fenofibrate is metabolized to fenofibric acid by plasma esterases; drug concentrations were determined using a validated HPLC method [12]. Pharmacokinetic parameters peak plasma concentration (Cmax), time to reach peak concentration (tmax), area under the curve (AUC), half-life (t½), and mean residence time (MRT) were derived by non-compartmental analysis using PK Solver 2.0.

Stability Study

The optimized formulation was subjected to accelerated and long-term stability studies according to ICH guidelines. Samples were stored at 25 ± 2°C/60 ± 5% RH and 40 ± 2°C/75 ± 5% RH for six months. At predetermined intervals (0, 1,2,3,4,5 and 6 months), formulations were evaluated for particle size, entrapment efficiency, cumulative drug release, and zeta potential to assess physicochemical stability.

Test Formulation for *In-Vivo* Pharmacological Evaluation

The optimized fenofibrate-loaded β-cyclodextrin nanosponge described above containing fenofibrate (100 mg), β-cyclodextrin (3.69 g), and diphenyl carbonate (0.80 g) per 100 mL batch, with a particle size of 183.42 nm, entrapment efficiency of 89.76%, and zeta potential of −29.88 mV was carried forward, without further modification, for evaluation of *in vivo* anti-inflammatory and lipid-modulating efficacy.

***In-Vivo* Pharmacological Evaluation: DSS-Induced Colitis Model**

Therapeutic efficacy was evaluated using a dextran sulfate sodium (DSS)-induced colitis model in male BALB/c mice (6–8 weeks old). Experimental colitis was induced by administering 3% DSS in drinking water for 7 days. Animals were divided into normal control, DSS control, fenofibrate suspension (100 mg/kg), and fenofibrate-loaded nanosponge (100 mg/kg, p.o., fenofibrate equivalent) groups and treated during days 8–17. The DSS-induced colitis model is widely used for evaluating intestinal inflammation, mucosal injury, and inflammatory responses in experimental colitis [14], with approval number 1414/A/11/CCSEA/NIPS/IAEC/2026/003. At the end of the treatment period, serum lipid parameters, including triglycerides, total cholesterol, HDL, LDL, and VLDL, were estimated. Colonic tissues were analyzed for inflammatory cytokines, including TNF-α, IL-1β, IL-6, and IL-10, followed by hematoxylin and eosin staining to evaluate mucosal damage, inflammatory-cell infiltration, crypt architecture, and goblet-cell preservation. The in-vivo experimental design and reporting were aligned with the recommendations of the ARRIVE 2.0 guidelines [11].

Statistical Analysis

Experimental data obtained from the Box–Behnken design were analyzed using Design-Expert® software. ANOVA was performed to determine the statistical significance of the developed quadratic models. Model adequacy was evaluated based on F-values, p-values, regression coefficients, and prediction errors. For the in-vivo pharmacological evaluation, group differences were analyzed by one-way ANOVA. Across both stages of the study, results are expressed as mean ± standard deviation, and statistical significance was considered at $p < 0.05$.

RESULTS

Evaluation of Nanosponges

Table 4. Box–Behnken Design for Fenofibrate Nanosponges

Run	A: Polymer conc. (%w/v)	B: Crosslinker:Polymer Ratio	C: Stirring time (h)	Particle size (nm)	Entrapment efficiency (%)	Drug release (%)	Zeta potential (mV)
1	4	2	6	245.2	78.2	82.54	−21.3
2	4	2	2	219.4	75.4	88.62	−18.7
3	2	4	2	198.0	82.1	85.32	−24.5
4	4	4	4	175.6	88.6	80.20	−29.1
5	6	6	4	265.9	90.2	72.45	−31.5
6	4	4	4	182.4	87.5	78.63	−27.8
7	4	4	4	178.2	89.1	79.41	−28.6
8	4	4	4	180.1	88.7	80.08	−28.9
9	6	2	4	255.7	84.3	76.83	−26.2
10	2	4	6	220.2	83.5	81.17	−25.4
11	6	4	6	235.4	86.2	77.46	−27.1
12	4	4	4	176.5	89.5	79.82	−29.4

13	4	6	6	230.6	91.3	73.21	−32.2
14	2	2	4	205.6	80.6	86.73	−22.8
15	2	6	4	240.5	92.5	71.60	−33.5
16	6	4	2	215.7	84.8	83.94	−24.9
17	4	6	2	225.9	88.9	78.08	−28

The Box–Behnken design comprised 17 experimental runs with polymer concentration (A), crosslinker:polymer ratio (B), and stirring time (C) as independent variables. Particle size, entrapment efficiency, drug release and zeta potential were evaluated as dependent responses.

Table 5. Consolidated ANOVA of Quadratic Models

Response	Significant terms ($p < 0.05$)	Most influential term	F-value	Model F-value	Model p-value
Particle size	A, C, A^2, B^2, C^2	B^2	77.02	19.61	0.0004
Entrapment efficiency	B, C^2	B	117.76	18.48	0.0004
Drug release	A, B, C, AB, B^2, C^2	B	362.26	75.51	<0.0001
Zeta potential	B, C, AB, C^2	B	209.64	33.40	<0.0001

The quadratic models for all four responses were statistically significant ($p \leq 0.0004$), indicating that the selected formulation and process variables adequately described the responses. For particle size, polymer concentration, stirring time and quadratic effects were significant, with B^2 showing the greatest influence ($F = 77.02$, $p < 0.0001$). Entrapment efficiency was primarily affected by the crosslinker:polymer ratio ($F = 117.76$, $p < 0.0001$), with a significant quadratic effect of stirring time. Drug release showed the strongest model dependence, with the crosslinker:polymer ratio as the dominant factor ($F = 362.26$, $p < 0.0001$), followed by stirring time. Zeta potential was also predominantly influenced by the crosslinker: polymer ratio ($F = 209.64$, $p < 0.0001$), together with stirring time and the A×B interaction.

Table 6. Quadratic Polynomial Equations for the Evaluated Responses

Response	Quadratic equation
Particle size (nm)	$178.20 + 13.385A + 5.63B + 10.25C - 6.25AB - 0.50AC - 7.50BC + 26.27A^2 + 36.77B^2 + 12.53C^2$
Entrapment efficiency (%)	$88.68 + 0.85A + 5.55B + 1.00C - 1.50AB + 0.00AC - 0.10BC - 0.54A^2 - 1.24B^2 - 3.99C^2$
Drug release (%)	$79.62 - 1.77A - 4.91B - 2.69C + 2.67AB - 0.58AC + 0.30BC - 0.69A^2 - 2.06B^2 + 3.04C^2$
Zeta potential (mV)	$-28.76 - 0.44A - 4.53B - 1.24C + 1.35AB - 0.33AC - 0.40BC - 0.08A^2 + 0.34B^2 + 3.37C^2$

The fitted quadratic equations describe the relationships between the three independent variables and the measured responses. The coefficients indicate the magnitude and direction of the individual, interaction and quadratic effects within the studied formulation space.

Natural Resources for Human Health
eISSN: 2583-1194

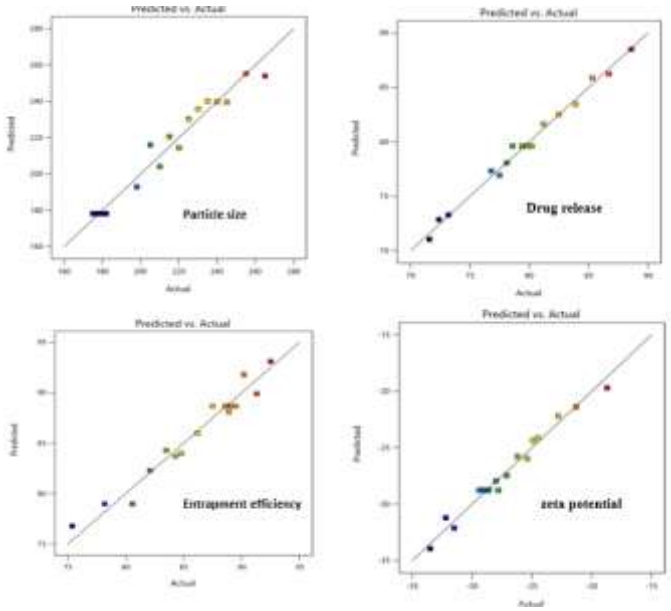

Figure 1. Predicted vs Actual plot

Table 7. Optimization and Validation of the Optimized Nanosponge Formulation

Response	Predicted	Observed	% Error	Within 95% CI
Particle size (nm)	181.66	183.42	0.97	Yes
Entrapment efficiency (%)	90.10	89.76	0.38	Yes
Drug release (%)	78.22	78.63	0.52	Yes
Zeta potential (mV)	−30.02	−29.88	0.47	Yes

Optimization was performed by targeting minimum particle size, maximum entrapment efficiency, 75–90% drug release at 10 h, and a zeta potential of −30 to −40 mV. The optimized formulation contained fenofibrate (100 mg), β-cyclodextrin (3.69 g), and diphenyl carbonate (0.80 g) per 100 mL batch. The optimized formulation showed close agreement between predicted and observed responses: prediction errors were below 1% for all responses, and all observed values fell within the 95% confidence intervals, confirming the predictive capability and robustness of the optimization model.

Table 8. Release Kinetics of the Optimized Formulation

Model	Result/interpretation
Zero-order	$R^2 \approx 0.909–0.915$; higher than first-order, indicating near-constant release.
First-order	$R^2 \approx 0.896–0.902$.
Higuchi	$R^2 \approx 0.794–0.802$.
Korsmeyer–Peppas	Highest R^2 values ($\approx 0.983–0.986$); n = 1.43–1.46.
Release mechanism	Super Case II transport; release attributed to polymer swelling and erosion.

Release kinetics indicated a higher R^2 for the zero-order model than the first-order model, suggesting near-constant release. The Korsmeyer–Peppas model exhibited the highest R^2 values, with n values of 1.43–1.46, corresponding to Super Case II

transport. Thus, drug release was predominantly associated with polymer swelling and erosion.

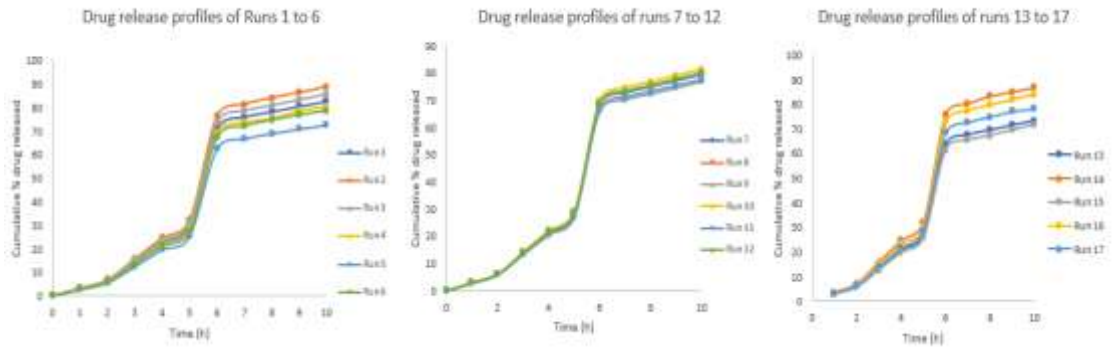

Figure 2. Drug release profiles of runs 1 to 17 (A = polymer concentration; B = crosslinker:polymer ratio; C = stirring time; AB = interaction between A and B; A^2, B^2 and C^2 = quadratic effects)

Optimization of Nanosponges

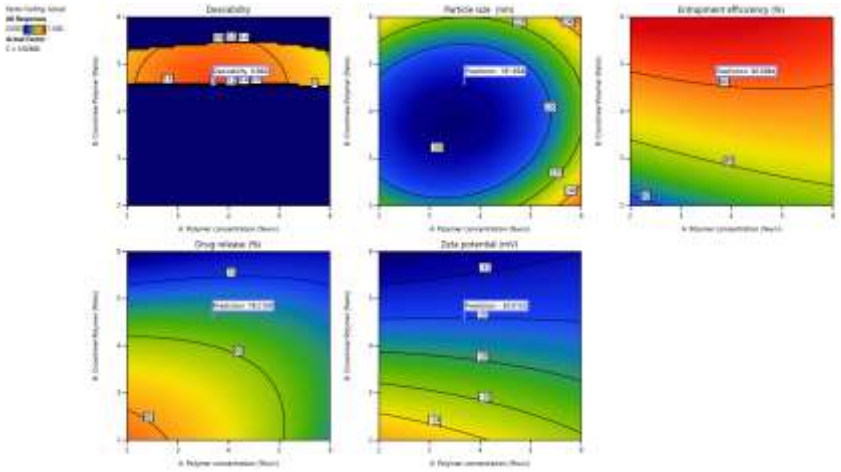

Figure 3. Solution for optimisation of nanosponges

The fenofibrate nanosponge formulation was optimized by setting response goals of lowest particle size, highest entrapment efficiency, drug release in 10 h of 75–90%, and zeta potential from −30 to −40 mV. One run with the highest desirability was obtained as the solution.

Table 9. Optimised Formulation Composition

Ingredient	Quantity per 100 mL batch
Fenofibrate	100 mg
β-Cyclodextrin	3.69 g
Diphenyl Carbonate	0.80 g
Ethanol	Q.s
Distilled Water	Q.s
Total Volume	100 mL

Particle Size of the Optimised Nanosponge Formulation

Natural Resources for Human Health
eISSN: 2583-1194

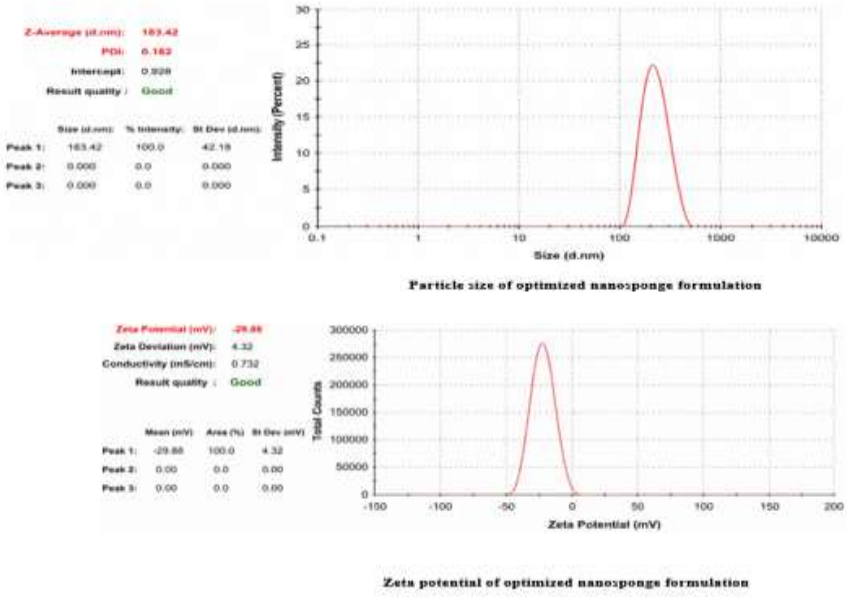

Figure 4. Particle size of optimised nanosponge formulation

Solubility and Dissolution Studies

The solubility of pure fenofibrate was 0.31 ± 0.01 µg/mL, whereas that of the optimised formulation was 3.87 ± 0.05 µg/mL. The β-cyclodextrin-based nanosponge formulation thus showed a 12-fold increase in aqueous solubility of the drug, an increase attributable to drug–water interaction through molecular inclusion [14]. The dissolution study similarly showed a significant difference between the pure drug and the optimised nanosponge formulation: only 12.48% of the pure drug was dissolved after 120 minutes, compared with 73.64% for the optimized nanosponge formulation (Figure 5).

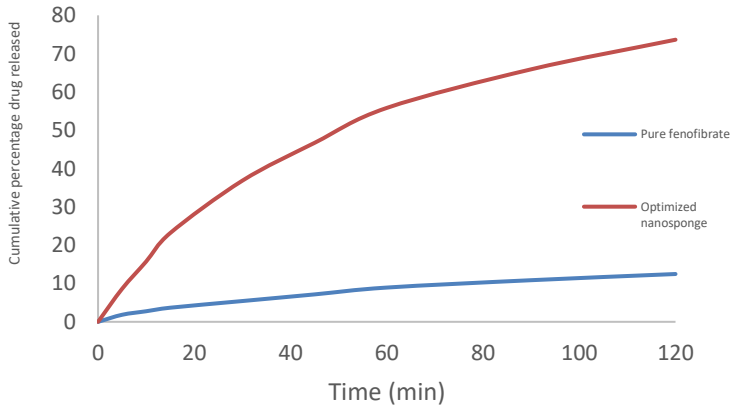

Figure 5. of dissolution studies of fenofibrate and optimized nanosponge formulation

Compatibility Studies

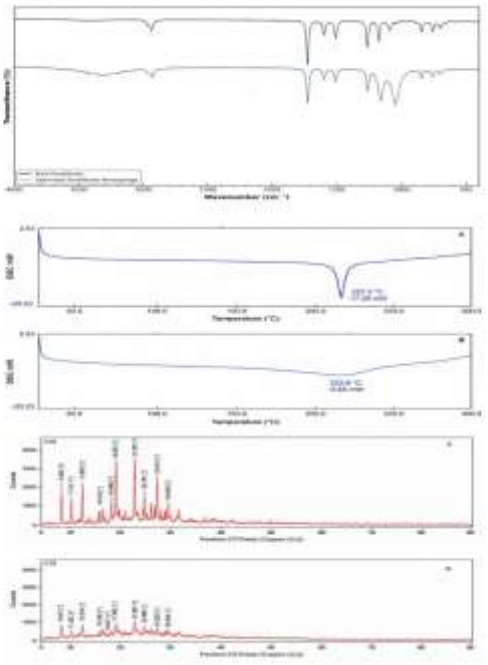

Figure 6. Compatibility studies (FTIR, DSC and XRD) of pure drug with optimized formulation

The FTIR spectrum of fenofibrate exhibited characteristic absorption peaks corresponding to its functional groups. A strong peak was observed at 1728 cm^{-1} corresponding to ester carbonyl (C=O) stretching vibration, and peaks in the 1600 and 1510 cm^{-1} regions corresponded to aromatic ring vibrations. In the optimised formulation, the characteristic peaks of the drug were retained, and a broad peak at 3300 cm^{-1} correlated with β-cyclodextrin. The thermogram of fenofibrate exhibited a sharp endothermic peak at 227.5°C (heat flow −17.29 mW), indicative of its crystalline nature. The thermogram of the optimised formulation exhibited a broader, less intense peak at 222.8°C (heat flow −3.85 mW), attributable to interactions between fenofibrate and the formulation components; reduced crystallinity of a poorly water-soluble drug such as fenofibrate may facilitate drug release from the formulation. The XRD pattern of the pure drug showed characteristic sharp peaks at 9.652°, 11.101°, 12.885°, 16.486°, 19.987°, 21.657°, 22.701°, 24.341° and 25.822°, confirming its crystalline nature. The optimised formulation contained peaks at 9.641°, 11.082°, 12.874°, 15.798°, 16.471°, 17.492°, 21.681°, 22.668°, 24.326° and 25.804°, of lower intensity, indicating reduced crystallinity following incorporation into the β-cyclodextrin nanosponge matrix.

Scanning Electron Microscopy

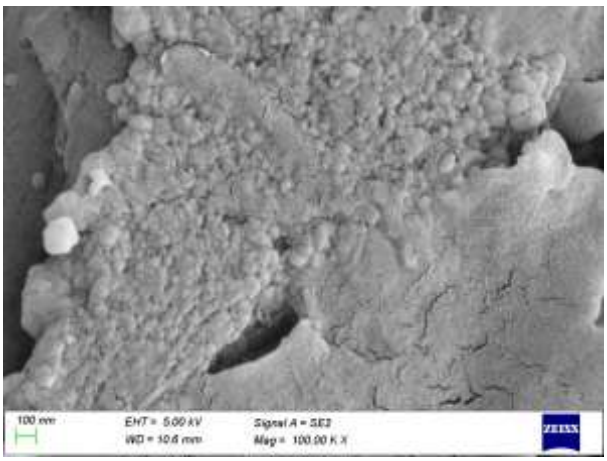

Figure 7. Scanning electron microscope image of optimized nanosponge formulation

The micrograph of the fenofibrate optimized nanosponge formulation showed a porous architecture with voids and interconnected pores, characteristic of nanosponges. The irregular and folded sponge-like network structure confirmed crosslinked nanosponge morphology. The surface was nonuniform, indicating internal porosity and matrix formation, with particles clustered as a result of the drying process.

***In-Vivo* Pharmacokinetic Studies**

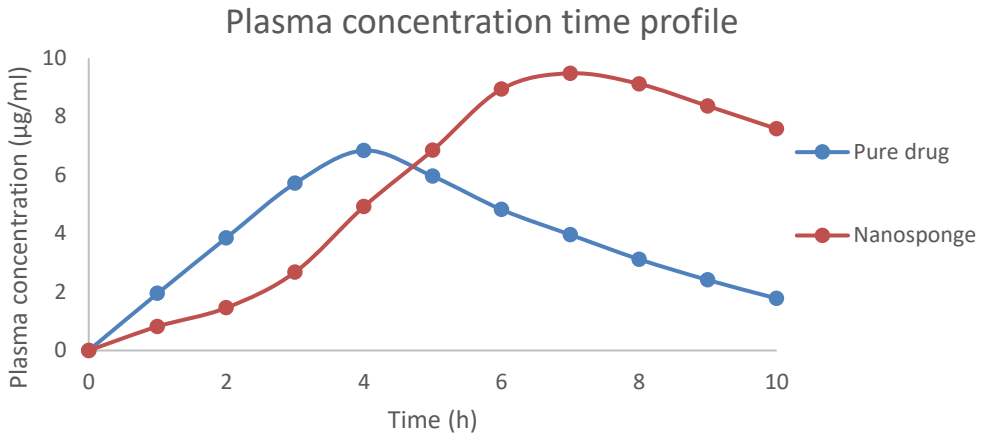

Figure 8. Plasma concentration–time profile of pure drug and nanosponge

Table 10. Pharmacokinetic Parameters of Pure Drug and Nanosponge

Parameter	Symbol (Unit)	Pure drug	Nanosponge
Peak plasma concentration	Cmax (µg/mL)	6.84	9.48
Time of peak plasma concentration	tmax (h)	4	7
Area under the curve (0–10 h)	AUC0–10 (µg·h/mL)	39.52	63.84
Area under the curve (0–∞)	AUC0–∞ (µg·h/mL)	44.10	72.35
Half-life	t1/2 (h)	3.21	5.86
Elimination rate constant	K (h^{-1})	0.216	0.118
Mean residence time	MRT (h)	4.82	7.96

The plasma concentration–time profile of the optimised formulation showed a lag phase during the initial hours, followed by an increase in drug concentration that reached a maximum at 7 h. Drug concentration was very low in the first two hours because of Eudragit S100, which is responsible for minimal drug release in acidic pH, with a gradual rise from 3 to 5 h. The delayed tmax reflects colon targeting, consistent with the pH-dependent solubility of the polymer. In contrast, the drug suspension showed rapid absorption with a tmax of 4 h, indicating a shorter duration of action. These results indicate that the nanosponge formulation achieved a sustained therapeutic effect.

Stability Studies

Table 11. Results of Stability Studies

Condition	Time (months)	Particle size (nm)	Entrapment efficiency (%)	Drug release (%)	Zeta potential (mV)
Room Temperature (25°C/60% RH)	0	183.42	89.76	78.63	−29.88
	1	184.55	89.35	78.20	−29.62

	2	185.68	88.94	77.77	−29.36
	3	186.81	88.53	77.34	−29.10
	4	187.94	88.12	76.91	−28.84
	5	189.07	87.71	76.48	−28.58
	6	190.20	87.30	76.05	−28.32
Accelerated Condition (40°C/75% RH)	0	183.42	89.76	78.63	−29.88
	1	185.85	89.05	77.82	−29.42
	2	188.28	88.34	77.01	−28.96
	3	190.71	87.63	76.20	−28.50
	4	193.14	86.92	75.39	−28.04
	5	195.57	86.21	74.58	−27.58
	6	198.00	85.50	73.77	−27.12

The optimised nanosponge formulation demonstrated good stability under both study conditions. No significant changes were observed in any of the four responses during the study period (Table 11). Slight changes under accelerated temperature and relative humidity may be attributable to polymer relaxation and particle aggregation.

Serum Lipid Profile in DSS-Induced Colitis

Table 12. Estimation of Serum Lipid Profile in DSS-Induced Colitis in Mice

Groups	Triglycerides (mg/dl)	Total cholesterol (mg/dl)	HDL (mg/dl)	LDL (mg/dl)	VLDL (mg/dl)
Normal Control	80.37 ± 1.8	127.8 ± 2.0	62.0 ± 1.96	49.5 ± 2.23	16.0 ± 0.98
DSS Control (3% DSS)	132.5 ± 3.0	241.8 ± 4.60	36.3 ± 1.32	179.0 ± 4.97	26.5 ± 0.65
Fenofibrate (100 mg/kg)	108.1 ± 2.31	176.8 ± 1.87	43.8 ± 2.14	96.9 ± 2.38	20.4 ± 1.65
Fenofibrate Nanosponge (100 mg/kg)	83.8 ± 2.67	133.0 ± 1.91	57.1 ± 1.96	59.2 ± 2.24	16.5 ± 0.59

$p > 0.05$ ns; $p < 0.001$; $p < 0.01$; $p < 0.05$, significance by two-way ANOVA with Bonferroni post-tests comparing treatment groups with the DSS control group; $p < 0.001$ # for comparison of the DSS control group with the normal control group.

The DSS control group exhibited significant dyslipidemia, characterized by increased triglycerides, total cholesterol, LDL, and VLDL levels, along with decreased HDL levels compared with the normal control group. Treatment with fenofibrate (suspension and nanosponge) significantly improved all lipid parameters. Fenofibrate restored the altered lipid profile in a dose-dependent manner, with the nanosponge formulation showing values closer to the normal control group, indicating a protective effect against DSS-induced lipid abnormalities.

Colonic Inflammatory Cytokines

Table 13. Estimation of Intestinal Inflammatory Mediators in DSS-Induced Colitis in Mice

Group	TNF-α (pg/mg tissue protein)	IL-1β (pg/mg tissue protein)	IL-6 (pg/mg tissue protein)	IL-10 (pg/mg tissue protein)
Normal Control	23.23 ± 3.13	21.29 ± 2.12	19.09 ± 2.7	60.67 ± 5.8
DSS Control (3% DSS)	97.12 ± 6.64	70.88 ± 4.23	88.81 ± 9.1	28.98 ± 3.4
Fenofibrate (100 mg/kg)	57.23 ± 2.22	39.47 ± 3.21	48.21 ± 5.1	39.54 ± 4.5
Fenofibrate Nanosponge (100 mg/kg)	30.26 ± 3.84	24.18 ± 2.56	27.89 ± 3.7	58.17 ± 5.2

$p > 0.05$ ns; $p < 0.001$; $p < 0.01$; $p < 0.05$, significance by two-way ANOVA with Bonferroni post-tests comparing treatment groups with the DSS control group; $p < 0.001$ # for comparison of the DSS control group with the normal control group.

The DSS control group showed a marked increase in the pro-inflammatory cytokines TNF-α, IL-1β, and IL-6, along with a significant reduction in the anti-inflammatory cytokine IL-10 compared with the normal control group, indicating severe intestinal inflammation. Treatment fenofibrate significantly reduced TNF-α, IL-1β, and IL-6 levels while increasing IL-10 levels, with the nanosponge groups producing the greatest effect, restoring cytokine levels close to normal control values and suggesting potent anti-inflammatory activity against DSS-induced colitis.

Histopathological Studies

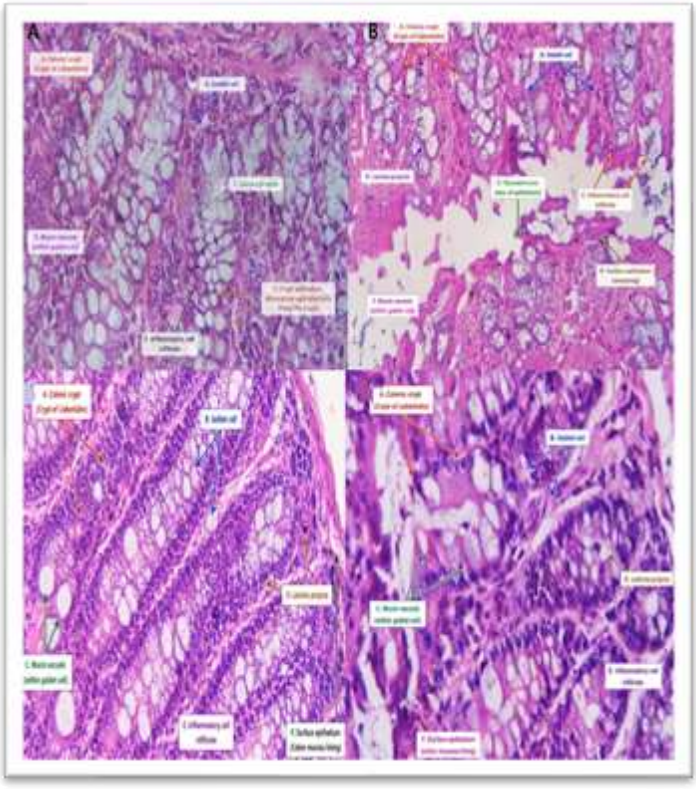

Figure 9. Histopathology of the colon in DSS-induced colitis in mice

A: The normal control group exhibited intact colonic mucosal architecture with well-organized crypts of Lieberkühn, abundant goblet cells, and preserved epithelial lining. B: The DSS control group showed marked mucosal injury characterized by crypt distortion, epithelial erosion, inflammatory cell infiltration, goblet cell depletion, and ulceration, indicative of severe colonic inflammation. C: Fenofibrate suspension demonstrated substantial protection against DSS-induced damage, with largely

preserved crypt architecture, abundant goblet cells, and only mild inflammatory cell infiltration. D: The fenofibrate nanosponge group (100 mg/kg) exhibited near-normal histological features with intact crypts, preserved epithelial lining, abundant mucin-producing goblet cells, and minimal inflammatory changes.

DISCUSSION

The present study was aimed at formulating a fenofibrate nanosponge to overcome its poor aqueous solubility and achieve colon-targeted drug delivery, and at evaluating whether this formulation strategy translates into meaningful anti-inflammatory efficacy in experimental colitis. Eudragit S100 was selected for its pH-dependent solubility profile, remaining intact at gastric pH and dissolving above pH 7 [13]. The crosslinker:polymer ratio was optimised to form a stable porous nanostructure, as excessive crosslinking can reduce pore size and drug diffusion, while insufficient crosslinking leads to structural instability. The optimised formulation showed a particle size of 183 nm, within the desirable nanoscale range; reduced particle size increases surface area, thereby improving dissolution and bioavailability of poorly soluble drugs, consistent with reports that nanosponge systems in the 100–500 nm range improve drug solubilization and permeability [5]. The increase in particle size with increasing polymer concentration is related to increased viscosity and reduced shear efficiency during formulation, leading to larger particles.

The entrapment efficiency of the optimized formulation was 90%, demonstrating effective drug incorporation within the nanosponge matrix. This can be related to the nanosponge's porous structure and hydrophobic interactions between fenofibrate and the polymer matrix that enhance drug retention; the unique cavity-based structure and higher surface area of nanosponges are key contributors to their high drug-loading capacity [15]. The in-vitro drug release studies indicated negligible drug release at acidic pH (1.2), minimal release at pH 6.8, and a significant increase at pH 7.4 followed by sustained release, confirming the effectiveness of the coated polymer in achieving colon-targeted delivery [16]. The initial lag phase in acidic conditions followed by release at alkaline pH ensures drug availability at the target site; the burst release may result from rapid polymer dissolution, followed by controlled release governed by diffusion from the nanosponge matrix. Drug release followed a non-Fickian mechanism, with a high R^2 for the Korsmeyer–Peppas model and an n value greater than one indicating that release results from a combination of polymer relaxation, swelling, and erosion rather than simple diffusion [17].

The zeta potential of the optimised formulation was −29.88 mV, indicating good physical stability, since values of $\geq \pm 30$ mV are generally considered sufficient to prevent aggregation [18]. The negative charge may arise from ionisation of carboxylic groups in the polymeric backbone, enhancing dispersion stability. Optimisation using Design-Expert software confirmed that polymer concentration, crosslinker:polymer ratio, and stirring time significantly influenced all four responses, and the close agreement between predicted and observed values confirmed the validity of the optimisation process [19].

The pharmacokinetic studies revealed that the optimized nanosponge formulation exhibited a significantly improved profile compared with the pure drug suspension [20]. The nanosponge showed a higher Cmax and delayed tmax, indicating controlled and site-specific drug release, while the higher AUC indicates enhanced oral bioavailability maintained by continued drug release from the nanosponge matrix. Scanning electron microscopy of the optimized formulation revealed a highly porous structure with an irregular, folded surface. The stability studies indicated no significant change in any response over the study period, demonstrating stability at both room and accelerated conditions, attributable to the crosslinked polymeric network that limits drug degradation and aggregation.

Building on this well-characterized, physicochemically stable and orally bioavailable colon-targeted platform, the in-vivo efficacy findings help clarify whether these formulation attributes translate into therapeutic benefit. DSS-induced colitis caused significant dyslipidemia, characterized by increased triglycerides, total cholesterol, LDL, and VLDL levels and decreased HDL levels, consistent with previous reports that intestinal inflammation and elevated cytokine production disrupt lipid metabolism. Treatment with fenofibrate significantly improved all lipid parameters, with the nanosponge formulation restoring values close to those of the normal control group. These results agree with studies demonstrating that fenofibrate activates PPAR-α, enhances fatty acid oxidation, reduces triglyceride synthesis, lowers LDL and VLDL levels, and increases HDL concentrations [21]. The observed lipid-lowering effect may also be attributed to the anti-inflammatory action of fenofibrate; previous studies have reported that fenofibrate suppresses inflammatory cytokines and improves metabolic abnormalities associated with colitis [22]. The present findings therefore suggest that fenofibrate effectively attenuates DSS-induced dyslipidemia through both lipid-regulating and anti-inflammatory mechanisms.

DSS administration significantly elevated the pro-inflammatory cytokines TNF-α, IL-1β, and IL-6 while reducing IL-10 levels, confirming induction of acute colonic inflammation. These findings are consistent with previous reports showing that DSS-induced epithelial barrier disruption activates macrophages and immune cells, resulting in excessive cytokine production and mucosal injury. Fenofibrate treatment significantly reduced TNF-α, IL-1β, and IL-6 levels and restored IL-10 levels, with the nanosponge formulation showing effects comparable to plain fenofibrate. Similar observations have been reported showing that fenofibrate attenuates experimental colitis through activation of PPAR-α and suppression of NF-κB-mediated inflammatory signaling [14], and that PPAR-α agonists more broadly reduce inflammatory cytokine expression and improve intestinal barrier integrity in colitis models [23]. The reduction in TNF-α and IL-6 observed in the present study is therefore likely associated with inhibition of NF-κB activation and decreased recruitment of inflammatory cells to the colonic mucosa.

Although free fenofibrate showed significant anti-inflammatory activity, its clinical application is limited by poor aqueous solubility, variable gastrointestinal absorption, and low local drug concentration at inflamed colonic sites. Incorporation of fenofibrate into the colon-targeted nanosponge system characterized in the first part of this study appears to overcome these limitations: nanosponges are porous nanocarriers capable of enhancing drug solubility, protecting the drug from premature degradation, and providing sustained release. For IBD specifically, fenofibrate-loaded nanosponges may offer additional advantages by enabling preferential accumulation at inflamed colonic tissue through increased mucosal adhesion and prolonged residence time. Sustained drug release from the nanosponge can maintain therapeutic concentrations at the site of inflammation while minimizing systemic exposure and dose-related adverse effects; the nanoscale size may also facilitate better penetration into inflamed tissue and enhanced cellular uptake by activated macrophages, leading to more effective suppression of inflammatory cytokines. Taken together with the pharmacokinetic and physicochemical advantages established for this formulation, a colon-targeted fenofibrate nanosponge system is expected to provide superior anti-inflammatory efficacy compared to conventional fenofibrate by improving solubility, enhancing local drug delivery, sustaining drug release, and maximizing PPAR-α-mediated therapeutic effects in inflammatory bowel disease. Such a strategy may reduce dosing frequency and improve patient compliance while offering a promising alternative for the management of ulcerative colitis.

CONCLUSION

Eudragit S100-based fenofibrate nanosponges were successfully developed as a colon-targeted delivery system using Box–Behnken design optimization, exhibiting nanoscale particle size, high entrapment efficiency, good stability, and a porous morphology. The formulation displayed pH-dependent, sustained drug release (78.63% at 10 h) and improved pharmacokinetic performance relative to pure drug suspension, with prediction errors below 1% confirming the robustness of the optimization model. In a DSS-induced colitis model in mice, this optimized colon-targeted formulation effectively corrected dyslipidemia reducing triglycerides, total cholesterol, LDL, and VLDL while elevating HDL likely via PPAR-α-mediated regulation of lipid metabolism and inflammation. The formulation also significantly attenuated colonic inflammation, evidenced by reduced pro-inflammatory cytokines (TNF-α, IL-1β, IL-6) and restored IL-10 levels, with near-normal preservation of colonic mucosal architecture on histopathology. These enhanced outcomes, achieved at doses comparable to or lower than plain fenofibrate, are attributable to the improved drug solubility, sustained release, and prolonged colonic residence established for this nanosponge platform. Collectively, these findings establish colon-targeted fenofibrate nanosponges as a promising, stable, and bioavailable strategy offering combined anti-inflammatory and lipid-modulating effects for inflammatory bowel disease management, together forming a complete evaluation of the platform's translational potential from formulation development to therapeutic proof-of-concept. Further preclinical and clinical investigations are needed to confirm long-term safety and translational potential.

Acknowledgements

None declared.

Author Contributions

APPROVED BY ALL AUTHORS.

Conflict of Interest

The authors declare no conflict of interest.

Ethical Approval

The pharmacokinetic study was reported as having ethical approval under IAEC: 1292/ac09/CPCSEA/2021/3.

AI Use Statement

Generative artificial intelligence tools were used solely to assist with language editing, grammar correction, and manuscript readability. The authors independently developed the study design, methodology, data analysis, interpretation of results, and scientific conclusions. AI tools were not used to generate, analyze, or fabricate experimental data. The authors take responsibility for the accuracy, originality, and integrity of the submitted manuscript.

REFERENCES

[1] Choi YE, Ngoc Nguyen HP, Khan N, et al. Enhanced oral delivery of fenofibrate using PEGylated solid lipid nanoparticles. J Pharm Investig. 2026. doi:10.1007/s40005-026-00813-6.

[2] Yang X, Guo H, Zou M. Inflammatory bowel diseases: pathological mechanisms and therapeutic perspectives. Mol Biomed. 2026;7(1):2. doi:10.1186/s43556-025-00395-z.

[3] Saez A, Herrero-Fernandez B, Gomez-Bris R, Sánchez-Martinez H, Gonzalez-Granado JM. Pathophysiology of inflammatory bowel disease: innate immune system. Int J Mol Sci. 2023;24(2):1526. doi:10.3390/ijms24021526.

[4] Noviello D, Amoroso C, Vecchi M, Facciotti F, Caprioli F. Curing inflammatory bowel diseases: breaking the barriers of current therapies—emerging strategies for a definitive treatment. Curr Opin Immunol. 2025;95:102593. doi:10.1016/j.coi.2025.102593.

[5] Garg A, Lai WC, Chopra H, Agrawal R, Singh T, Chaudhary R, Dubey BN. Nanosponge: a promising and intriguing strategy in medical and pharmaceutical science. Heliyon. 2024;10(1):e23303. doi:10.1016/j.heliyon.2023.e23303.

[6] Salazar Sandoval S, Cortés-Adasme E, Gallardo-Toledo E, Araya I, Celis F, Yutronic N, Jara P, Kogan MJ. β-Cyclodextrin-based nanosponges inclusion compounds associated with gold nanorods for potential NIR-II drug delivery. Pharmaceutics. 2022;14(10):2206. doi:10.3390/pharmaceutics14102206.

[7] Yeung C, McCoubrey LE, Basit AW. Advances in colon-targeted drug technologies. Curr Opin Gastroenterol. 2025;41(1):9–15. doi:10.1097/MOG.0000000000001064.

[8] Pannala VR, Balik-Meisner MR, Mav D, Phadke DP, Scholl EH, Shah RR, Casey W, Auerbach SS, Wallqvist A. Fenofibrate differentially activates PPARα-mediated lipid metabolism in rat kidney and liver. Sci Rep. 2025;15(1):36842. doi:10.1038/s41598-025-20731-1.

[9] Gallucci GM, Alsuwayt B, Auclair AM, et al. Fenofibrate downregulates NF-ϰB signaling to inhibit pro-inflammatory cytokine secretion in human THP-1 macrophages and during primary biliary cholangitis. Inflammation. 2022;45:2570–2581. doi:10.1007/s10753-022-01713-1.

[10] Cooper HS, Murthy S, Kido K, Yoshitake H, Flanigan A. Dysplasia and cancer in the dextran sulfate sodium mouse colitis model. Relevance to colitis-associated neoplasia in the human: a study of histopathology, β-catenin and p53 expression and the role of inflammation. Carcinogenesis. 2000;21(4):757–768. doi:10.1093/carcin/21.4.757.

[11] Percie du Sert N, Hurst V, Ahluwalia A, Alam S, Avey MT, Baker M, et al. The ARRIVE guidelines 2.0: updated guidelines for reporting animal research. PLoS Biol. 2020;18(7):e3000410. doi:10.1371/journal.pbio.3000410.

[12] Xu Y, Wang Y, Li XM, Huang Q, Chen W, Liu R, Chen BA, Wei P. Study on the release of fenofibrate nanosuspension in vitro and its correlation with in situ intestinal and in vivo absorption kinetics in rats. Drug Dev Ind Pharm. 2014;40(7):972–979. doi:10.3109/03639045.2013.794828.

[13] Heikal EJ, Kaoud RM, Gad S, Mokhtar HI, Alattar A, Alshaman R, Zaitone SA, Moustafa YM, Hammady TM.

Development of novel pH-sensitive Eudragit-coated beads containing curcumin-mesalamine combination for colon-specific drug delivery. Gels. 2023;9(4):264. doi:10.3390/gels9040264.

[14] Qi Y, Jiang C, Tanaka N, Krausz KW, Brocker CN, Fang ZZ, Bredell BX, Shah YM, Gonzalez FJ. PPARα-dependent exacerbation of experimental colitis by the hypolipidemic drug fenofibrate. Am J Physiol Gastrointest Liver Physiol. 2014;307(5):G564–G573. doi:10.1152/ajpgi.00153.2014.

[15] Shrestha S, Bhattacharya S. Versatile use of nanosponge in the pharmaceutical arena: a mini-review. Recent Pat Nanotechnol. 2020;14(4):351–359. doi:10.2174/1872210514999200901200558.

[16] Badusha SA, Reddy JRK. Nanosponges: a comprehensive analysis on drug delivery systems for the treatment of diverse diseases. Next Nanotechnol. 2026;9:100442. doi:10.1016/j.nxnano.2026.100442.

[17] Herdiana Y, Wathoni N, Shamsuddin S, Muchtaridi M. Drug release study of the chitosan-based nanoparticles. Heliyon. 2022;8(1):e08674. doi:10.1016/j.heliyon.2021.e08674.

[18] Németh Z, Csóka I, Semnani Jazani R, Sipos B, Haspel H, Kozma G, Kónya Z, Dobó DG. Quality by design-driven zeta potential optimisation study of liposomes with charge imparting membrane additives. Pharmaceutics. 2022;14(9):1798. doi:10.3390/pharmaceutics14091798.

[19] Krzywanski J, Sosnowski M, Grabowska K, Zylka A, Lasek L, Kijo-Kleczkowska A. Advanced computational methods for modeling, prediction and optimization—a review. Materials. 2024;17(14):3521. doi:10.3390/ma17143521.

[20] Gaber DA, Radwan MA, Alzughaibi DA, Alail JA, Aljumah RS, Aloqla RM, Alkhalifah SA, Abdoun SA. Formulation and evaluation of piroxicam nanosponge for improved internal solubility and analgesic activity. Drug Deliv. 2023;30(1):2174208. doi:10.1080/10717544.2023.2174208.

[21] Lakhia R, Yheskel M, Flaten A, Quittner-Strom EB, Holland WL, Patel V. PPARα agonist fenofibrate enhances fatty acid β-oxidation and attenuates polycystic kidney and liver disease in mice. Am J Physiol Renal Physiol. 2018;314(1):F122–F131. doi:10.1152/ajprenal.00352.2017.

[22] Alarfaj SJ, Bahaa MM, Elmasry TA, Elberri EI, El-Khateeb E, Hamouda AO, Salahuddin MM, Kamal M, Gadallah ANAA, Eltantawy N, Yasser M, Negm WA, Hamouda MA, Alsegiani AS, Alrubia S, Eldesoqui M, Abdallah MS. Fenofibrate as an adjunct therapy for ulcerative colitis: targeting inflammation via SIRT1, NLRP3, and AMPK pathways: a randomized controlled pilot study. Drug Des Devel Ther. 2024;18:5239–5253. doi:10.2147/DDDT.S490772.

[23] Bashiri K, Mattar MC, Meighani A, Mason AL. Peroxisome proliferator-activated receptors in inflammatory bowel disease: linking immunometabolism, lipid signaling, and therapeutic potential. Intest Res. 2026;24(1):11–26. doi:10.5217/ir.2025.00090.